c-MYC is an aggregation-prone, amyloidogenic protein

Ling Lin[1], Kun-Han Chuang[1,2], and Chengkai Dai[1,6,*]

[1]Mouse Cancer Genetics Program, Center for Cancer Research, National Cancer Institute, Frederick, MD 21702, USA

[2]Current address: School of Basic Medical Sciences, Fujian Medical University, Fuzhou, Fujian 350108, China

[6]Lead contact

* Correspondence: chengkai.dai@nih.gov

SUMMARY

As a master transcription factor, c-MYC governs a plethora of biological processes. Despite being a prominent oncoprotein, counterintuitively, c-MYC also possesses an intrinsic tumor suppressor activity through induction of apoptosis, a phenomenon known as "the paradox of c-MYC". Serendipitously, we discover that c-MYC is aggregation-prone, becoming detergent-insoluble upon heat shock. Even in the absence of heat shock, c-MYC assembles into soluble oligomers exhibiting characteristics of amyloids in both human cancer tissues and, surprisingly, human Alzheimer's disease brains. *In vitro*, recombinant c-MYC proteins form amyloid oligomers as well as protofibrils spontaneously. By contrast, its obligate dimerization partner MAX is non-amyloidogenic and, moreover, antagonizes the amyloidogenesis of c-MYC. Screening of the c-MYC synthetic peptide library identifies two intrinsically disordered short linear fragments, which are amyloidogenic *in vitro*. This amyloidogenesis of c-MYC, importantly, induces apoptosis largely independently of transcription. Thus, our findings unveil a previously unrecognized amyloidogenicity of c-MYC, which may contribute to its tumor-suppressing activity. Upon loss of the stringent control of its expression, conceptually, this amyloidogenesis of c-MYC may serve as a built-in failsafe mechanism to self-destruct its troublesome oncogenic potential.

INTRODUCTION

The bHLH/ZIP transcription factor c-MYC plays vital roles in human biology, particularly acting as an oncogenic driver and a pluripotency-reprogramming factor.[1,2] Through interaction with MYC-associated factor X (MAX), MYC/MAX dimers bind to the canonical E-box (5'-CACGTG-3') element or its variants and regulate the transcription of 10-15% of the human genome.[1,3] It is generally believed that dimerization with MAX is a prerequisite for the transcriptional activity of c-MYC.[4] Unlike in primary, non-transformed cells, where its protein undergoes rapid turnover and remains at low levels, c-MYC expression is invariably elevated in human cancers, due to gene amplification, translocation, or protein stabilization.[5] Despite being a prominent oncoprotein, paradoxically, c-MYC can elicit apoptosis, an intrinsic tumor-suppressing activity, especially under stressed conditions or with abundant expression.[6,7] This induction of apoptosis, unsurprisingly, has been ascribed to its transcriptional action.[8,9]

Proteins including c-MYC naturally remain functional at the soluble and folded state; however, proteotoxic stressors and genetic mutations can cause protein misfolding and aggregation, leading to loss of function and cytotoxicity. Amyloids, a rare form of aggregates enriched with cross-β-sheet structures, have been closely implicated in human diseases particularly neurodegenerative disorders.[10] Two fluorescence dyes, Congo red (CR) and thioflavin T (ThT), have been extensively applied to detect amyloids through physical binding.[11] In addition, the conformation-specific antibody A11 has become an invaluable tool for recognizing the soluble prefibrillar amyloid oligomers (AOs), a conformer highly toxic to neurons, independently of primary amino acid sequences.[12] Beyond detection, CR has been known to impede the amyloidogenic process.[13,14]

Serendipitously, our studies now discover that c-MYC, but not its obligate dimerization partner MAX, proteins become detergent-insoluble aggregates upon heat shock (HS). Furthermore, in human cancer tissues and, surprisingly, Alzheimer's disease (AD) brains c-MYC assembles into detergent-soluble oligomers captured by the A11 antibody even in the absence of HS. Interestingly, this aggregation and oligomerization can be blocked by CR. *In vitro*, recombinant c-MYC, but not MAX, proteins spontaneously form AOs as well as protofibrils, demonstrating the intrinsic amyloidogenicity of c-MYC. MAX, intriguingly, prevents the amyloidogenesis of c-MYC. By screening a synthetic peptide library of human c-MYC, two intrinsically disordered short linear fragments (aa20-39 and aa210-228) are identified to be amyloidogenic. Moreover, a large majority of amino acids within these two fragments contribute to their amyloidogenicity, revealed by alanine scan. Unexpectedly, the transcription-deficient c-MYC mutant, which lacks the C-terminal MAX-dimerizing and DNA-binding domain, can still induce apoptosis. Deletion of these two amyloidogenic regions, importantly, largely blocks this apoptosis. Taken together, our data pinpoint c-MYC as an aggregation-prone, amyloidogenic protein. Biologically, the amyloid state of c-MYC prompts apoptosis independently of transcription, fully unleashing its tumor-suppressing potential. Thus, our findings both provide new insights into the paradox of c-MYC and uncover its complex implications in human pathologies, including cancer and neurodegeneration.

RESULTS

c-MYC acquires amyloid-like attributes under stressed and pathological conditions

We recently discovered that under non-stressed conditions heat shock factor 1 (HSF1) potentiates the c-MYC-mediated transcription via physical interactions, a non-canonical transcriptional action of HSF1.[15] Subsequently, we were curious about how this c-MYC–HSF1 interaction is affected by proteotoxic stress, such as HS, wherein HSF1 is obligatory for initiating the canonical heat-shock, or proteotoxic stress, response (HSR/PSR).[16,17]

In HeLa cells transient HS, unexpectedly, caused a notable reduction in detergent-soluble c-MYC proteins, accompanied with an increase in detergent-insoluble proteins (Figure 1A). This transition in physical states suggests c-MYC aggregation upon proteotoxic stress. By sharp contrast, its obligate dimerization partner MAX did not aggregate. Neither did major cellular chaperones including HSP90 and HSC/HSP70 (Figure 1A), which are much more abundant than c-MYC inside cells. Of note, this c-MYC aggregation was partially blocked by CR (Figure 1A). Despite being a popular amyloid stain known to impede amyloidogenesis, CR may also counteract generic protein aggregation. To determine whether c-MYC could form amyloid-like aggregates, we took advantage of the conformation-specific A11 antibody, which has been widely applied to recognize soluble prefibrillar AOs.[12] In HeLa cells, A11 antibodies precipitated both exogenous HA-c-MYC and endogenous c-MYC proteins in the absence of HS (Figures 1B and 1C). This finding was further confirmed by *in situ* Proximity Ligation Assay (PLA), [18] a technique detecting protein-protein interactions or two distinct epitopes located on the very same protein, in cultured HeLa cells (Figure 1D). The PLA signals were quantitated by flow cytometry (Figure S1A). Of note, these PLA signals were largely localized in the cytoplasm (Figure 1D),

114 suggesting that these special c-MYC conformers are incompetent at transcription. The
115 emergence of such conformers is not due to cell culture artifacts, as these A11^{+}-c-MYC
116 oligomers were readily detected in human cancer tissues, both primary and xenografted (Figures
117 1E, 1F, and S1B). Intriguingly, such c-MYC oligomers were also detected in human AD brain
118 tissues (Figure 1G), resembling diffuse Aβ plaques. Importantly, the genesis of A11^{+}-c-MYC
119 oligomers was blocked by CR treatment (Figures 1H and S1C), further corroborating the
120 amyloidogenic nature of such aggregates. Together, these findings support that c-MYC proteins,
121 at least under proteotoxic stress and certain pathological conditions, could demonstrate some
122 characteristics of amyloids.

123

124 **c-MYC is intrinsically amyloidogenic**

125 It is worth pointing out that both the immunoprecipitation and PLA staining only indicate that
126 either c-MYC interacted with AOs or c-MYC itself became amyloids. To distinguish these two
127 possibilities, we next resorted to *in vitro* assays using purified recombinant proteins.

128

129 In the classic *in vitro* fibrillation assay, recombinant c-MYC proteins, prepared by two
130 independent sources, spontaneously assembled into amyloid fibrils, detected by ThT binding
131 (Figure 2A). This sharply contrasted with GST and a panel of recombinant transcription factors
132 including HSF1, USF1, OCT4, as well as MAX (Figure 2A). Of note, neither MAX, the obligate
133 dimerization partner of c-MYC, nor USF1, another member of the c-MYC family, formed
134 amyloid fibrils, underlining the specific amyloidogenicity of c-MYC. Aside from amyloid fibrils,
135 recombinant c-MYC proteins also assembled into soluble AOs, recognized by the A11 antibody

136 (Figure 2B). Likely due to the solubilizing effect of GST tags, GST-c-MYC proteins produced
137 markedly more AOs. Transmission electron microscopy (TEM) further confirmed the assembly
138 of protofibrils from recombinant c-MYC proteins (Figure 2C). Collectively, these *in vitro* studies
139 indicate that c-MYC itself is an amyloidogenic protein.

140

141 Considering that c-MYC dimerizes with non-amyloidogenic MAX under physiological
142 conditions,[4] we were intrigued by the question of how this dimerization impacts the
143 amyloidogenesis of c-MYC. First, the *in vitro* fibrillation assay revealed that recombinant c-
144 MYC/MAX heterodimers did not form amyloid fibrils, in stark contrast to recombinant c-MYC
145 proteins alone (Figures 2D and 2E). Second, disruption of the MYC/MAX dimerization in HeLa
146 cells using the small molecule 10058-F4 led to increased $A11^{+}$–c-MYC oligomers, despite
147 reduced soluble c-MYC proteins (Figures 2F, S2A, and S2B).[19] These findings together strongly
148 support that dimerization with MAX suppresses the amyloidogenesis of c-MYC.

149

150 **Deciphering the intrinsic amyloidogenicity of c-MYC**

151 To systematically dissect the amyloidogenic regions, we designed a synthetic peptide library of
152 human c-MYC proteins, each peptide encompassing 19 non-overlapping amino acids. This
153 technique has been successfully applied to delineate protein-protein interaction interfaces
154 previously.[15] Among total 24 linear peptides, only two, P2 (aa20-38) and P12 (aa210-228),
155 displayed evident amyloidogenesis, like the full-length c-MYC protein, indicated by the *in vitro*
156 fibrillation assay (Figure 3A). Of interest, only P12 consistently assembled into $A11^{+}$-AOs as

157 well (Figure 3B). It is noteworthy that both P2 and P12 are located within the intrinsically
158 disordered regions (IDRs) of c-MYC (Figure S3A).

159

160 To further pinpoint individual amino acids critical to this amyloidogenicity, both P2 and P12
161 were subjected to alanine scan. Revealed by *in vitro* fibrillation assays, in most cases mutation of
162 individual amino acids markedly diminished amyloid fibrillation (Figures 3C and 3D). These
163 findings indicate that intrinsically disordered short linear fragments can serve as the
164 amyloidogenic regions. Furthermore, it appears that numerous residues within these regions
165 collectively contribute to the amyloidogenicity.

166

167 **Illustrating the biological implications of c-MYC amyloidogenesis**

168 Aggregates, especially amyloids, are cytotoxic. We reasoned that the amyloidogenesis of c-MYC
169 might cause apoptosis, contributing to its tumor-suppressing effect. It has been well documented
170 that c-MYC can trigger apoptosis under stressed conditions, including serum starvation and DNA
171 damage, or simply with elevated expression. [6-9] To distinguish the transcription-induced from
172 amyloid-induced apoptosis, we generate the transcription-deficient HA-c-MYC$^{\Delta C}$ mutant, which
173 lacks the C-terminal DNA-binding and MAX-dimerizing domains but retains the amyloidogenic
174 regions (Figure 4A). Overexpression of HA-c-MYC^{WT}, as expected, induced apoptosis in serum-
175 starved NIH-3T3 cells, detected by caspase 3 cleavage (Figures 4B). So did HA-c-MYC$^{\Delta C}$
176 mutants (Figures 4B), suggesting a surprising transcription-independent mechanism. Naturally,
177 we asked whether the amyloidogenesis of HA-c-MYC$^{\Delta C}$ contributes to this apoptosis. To this
178 end, the two amyloidogenic regions were deleted from HA-c-MYC$^{\Delta C}$. Of note, deletions of these

179 regions altered the expression of HA-c-MYC$^{\Delta C}$ (Figure 4C). The apoptosis-inducing effects were
180 normalized by their expression levels accordingly. While deletion of the P2 region markedly
181 diminished apoptosis, deletion of the P12 region was less effective (Figure 4D). Of note, deletion
182 of the amyloidogenic regions did not further impair the residual transcriptional activity of HA-c-
183 MYC$^{\Delta C}$ mutants (Figure 4A); by contrast, it did significantly diminish the apoptosis-inducing
184 capability of these mutants (Figure 4D), decoupling apoptosis induction from transcriptional
185 activity. In aggregate, these findings strongly support that the amyloidogenesis of c-MYC
186 provokes cytotoxicity, which could contribute to its intrinsic tumor suppressor activity.

187

188

189

190

191

192

193

194

195

196

197

198

199 **DISCUSSION**

200 **c-MYC is an aggregation-prone and amyloidogenic protein**

201 Our combined *ex vivo* and *in vitro* studies provide compelling evidence pinpointing c-MYC as an
202 aggregation-prone and amyloidogenic protein. This conclusion is drawn from multiple
203 independent lines of evidence, including the blockade of c-MYC amyloidogenesis by CR, ThT
204 binding of c-MYC amyloid fibrils, recognition of c-MYC AOs by A11 antibodies, as well as
205 direct visualization of c-MYC amyloid protofibrils by TEM. Most importantly, we have
206 delineated two intrinsically disordered short linear fragments as the amyloidogenic regions.
207 Although both short fragments assembled into amyloid fibrils *in vitro*, indicated by ThT binding,
208 only one of them, P12, consistently produced $A11^{+}$–AOs. It remains possible that P2 may
209 assemble into a distinct class of AOs, which cannot be recognized by the A11 antibody.

210

211 **MAX acts as a suppressor of c-MYC amyloidogenesis**

212 One intriguing discovery is that its obligate dimerization partner MAX, which is non-
213 amyloidogenic, antagonizes the amyloidogenesis of c-MYC. This finding predicts that in
214 primary, non-transformed cells, where c-MYC levels remain low and sufficient MAX is
215 available for dimerization, the amyloidogenesis of c-MYC would be curtailed. However, a vastly
216 different scenario would be expected in cancerous cells, where c-MYC levels are markedly
217 elevated and, importantly, the expression of *c-MYC* and *MAX* are poorly correlated (Figures S4A,
218 S4B, and S4C). Conceivably, c-MYC is selected for overexpression owing to its oncogenic
219 potential; by contrast, MAX is not subjected to the same selection pressure, owing to its tumor-
220 suppressing effects through dimerization with MXD family proteins. [20,21] This disproportionate

221 c-MYC and MAX expression, likely, unleashes the amyloidogenesis of c-MYC in human
222 cancers.

223

224 **New insights into the paradox of c-MYC**

225 "The paradox of c-MYC" depicts an intriguing dichotomy, in which c-MYC acts as an
226 oncoprotein with intrinsic tumor suppressor activity. This stimulation of apoptosis, traditionally,
227 has been exclusively ascribed to the transcriptional action of c-MYC. Our studies now reveal that
228 the amyloid state of c-MYC provokes apoptosis in a largely transcription-independent fashion.
229 Thus, c-MYC can exert its tumor suppressor activity via both transcription-dependent and -
230 independent mechanisms, likely contingent upon the cellular c-MYC abundance. Given its
231 fundamental roles in biology, unsurprisingly, the expression of c-MYC is subjected to
232 exceedingly tight control under physiological conditions, loss of which would inevitably lead to
233 pathogeneses particularly malignancy. Conceptually, this amyloidogenic process could serve as a
234 built-in failsafe mechanism for c-MYC to self-destruct its troublesome oncogenic potential.

235

236 **Implications of c-MYC amyloidogenesis in cancer and neurodegeneration**

237 Previously, we uncovered the phenomenon of "tumor-suppressive amyloidogenesis", [14] owing to
238 widespread proteomic instability of cancer. Now, our findings further pinpoint c-MYC as an
239 exemplar of tumor-associated amyloids. Given their cytotoxic impact, these amyloid conformers
240 of c-MYC must be contained to avert their tumor-suppressing effects in cancerous cells. Our
241 previous study revealed that HSF1, the master regulator of the HSR/PSR, could physically
242 neutralize toxic AOs. [22] Intriguingly, HSF1 happens to interact with c-MYC. [15] Thus, in

243 cancerous cells HSF1 may help counteract these c-MYC amyloids. In accordance with this
244 notion, the expression of *HSF1* and *c-MYC* is well correlated in human cancers.[15]
245
246 Beyond cancer, our data unveil that the amyloidogenesis of c-MYC manifests in human AD as
247 well. In fact, it has been reported that MYC expression is elevated in human AD brains.[23,24]
248 Moreover, overexpression of *c-MYC* in neurons led to neurodegeneration in mice, an effect
249 attributed to neuronal cell cycle re-entry. [25] Our findings, nevertheless, suggest an implication of
250 c-MYC amyloidogenesis in neurodegenerative disorders, a notion warranting further
251 investigations.
252
253
254
255
256
257
258
259
260
261
262

Acknowledgments

This research was supported by the Intramural Research Program of the National Institutes of Health (NIH), National Cancer Institute, Center for Cancer Research (1ZIABC011767). The contributions of the NIH authors are considered Works of the United States Government. The findings and conclusions presented in this paper are those of the authors and do not necessarily reflect the views of the NIH or the U.S. Department of Health and Human Services.

Author contributions: L. L., K-H. C., and C. D. designed and conducted the experiments. C.D. conceptualized and supervised this study and analyzed the results. C.D. wrote the manuscript.

Declaration of interests: The authors declare no competing interests.

EXPERIMENTAL METHODS

Cell Lines and Reagents

HeLa (female) cells and NIH3T3 (male) cells were purchased from ATCC. They were authenticated by ATCC by STR profiling. All cell cultures were maintained in DMEM supplemented with 10% HyClone bovine growth serum and 1% penicillin–streptomycin. Cells were maintained in an incubator with 5% CO2 at 37 °C. All cell lines were routinely tested for mycoplasma contamination using MycoAlert Mycoplasm Detection kits.

Recombinant proteins were all purchased commercially, including c-MYC/MAX complexes (cat#81087, Active Motif Inc.), His-HSF1 (cat#ADI-SPP-900-F, Enzo Life Sciences Inc.), GST-c-MYC (cat#M86-30G, Sino Biological US Inc.), His-c-MYC (cat#230-00580-100, RayBiotech Inc.), GST (cat#G52-30U-50, SignalChem Inc.), His-GST (cat#RPT0002, ABclonal Inc.), His-MAX (cat#81017, Active Motif Inc.), His-USF1 (cat#228-21891-2, RayBiotech Inc.), and His-OCT4 (cat#228-21139-2, RayBiotech Inc.).

All antibodies were purchased commercially, including rabbit polyclonal anti-amyloid oligomer (A11) Ab (cat#SPC-506, StressMarq Biosciences Inc.), rabbit monoclonal anti-c-MYC/N-MYC (D3N8F) Ab (cat#13987, Cell Signaling Technology), rabbit monoclonal ani-MAX (E6F6Y) Ab (cat#17471, Cell Signaling Technology), mouse monoclonal anti-HSC/HSP70 (W27) Ab (cat#sc-24, Santa Cruz Biotechnology Inc.), mouse monoclonal anti-HSP90α/β (F-8) Ab (cat#sc-13119, Santa Cruz Biotechnology Inc.), rabbit monoclonal anti-cleaved caspase 3 (Asp175) (D3E9) Ab (cat#9579, Cell Signaling Technology), goat polyclonal anti-c-MYC Ab (cat#AF3696, R&D

Systems Inc.), mouse monoclonal anti-HA Ab (cat#901513, BioLegend Inc.), mouse monoclonal anti-βActin (GT5512) Ab (cat#GTX629630, GeneTex Inc.), normal rabbit IgG (cat#02-6102,ThermoFisher Scientific Inc.), Peroxidase AffiniPure Goat Anti-Rabbit IgG (H+L) (cat#111-035-144, Jackson ImmunoResearch Inc.), Peroxidase AffiniPure Goat Anti-Mouse IgG (H+L) (cat#115-035-003, Jackson ImmunoResearch Inc.), and Peroxidase IgG Fraction Monoclonal Mouse Anti-Goat IgG, light chain specific (cat#205-032-176, Jackson ImmunoResearch Inc.).

All chemicals were purchased commercially, including Thioflavin T (ThT) (cat# AC211760050, ThermoFisher Scientific Inc.), Congo red (CR) (cat#C580-25, ThermoFisher Scientific Inc.), Janus Green B (cat# AC191680050, Fisher Scientific LLC), and 10058-F4 (cat#T3048, TargetMol Chemicals Inc.).

pcDNA-GFP and pcDNA3-2xHA-MYC were gifts from Martine Roussel (Addgene plasmid#74165 and 74164, respectively). pcDNA3-2xHA-MYC$^{\Delta C}$, 2xHA-MYC$^{\Delta C+\Delta P2}$, 2xHA-MYC$^{\Delta C+\Delta P12}$, and 2xHA-MYC$^{\Delta C+\Delta P2+\Delta P12}$ were generated using the Q5 Site-Directed Mutagenesis kit (cat#E0554S, New England Biolabs Inc.). pMYC-SEAP was purchased from Clontech Laboratories (Cell signaling pathway profiling systems, cat#631910) and pCMV-Gaussia Luc was purchased from Thermo Fisher Scientific (cat#16147).

The c-MYC peptide library and alanine scan libraries were custom synthesized by GenScript USA Inc.

Paraffin sections of human liver cancer (cat#HuCAT081) and prostate cancer (cat#HuCAT371) were purchased from TissueArray.com LLC. Paraffin sections of human Alzheimer's disease brains (cat#CSA0225P) were purchased from American MasterTech Scientific. Paraffin sections of human A2058 melanomas were prepared from xenografted tumors described previously. [14]

Soluble and Insoluble Fractionation

HeLa cells were treated with Congo red for 24 hours, followed by incubation at 43°C for 30 min. Cells were then trypsinized, washed, and resuspended in 1xPBS for cell counting. Equal numbers of cells were used for soluble and insoluble fractionation. The detailed procedures were described previously. [22]

In-Cell PLA ELISA

To avoid the interference of CR or 10058-F4 in PLA fluorescence detection, In-Cell PLA ELISA was adopted using the Duolink® In Situ Detection Reagent Brightfield (cat#DUO92012, Sigma-Aldrich). The detailed procedures were described previously.[15] HeLa cells were seeded in 96-well culture plates (7000 cells/well) and treated with CR for 24 hr or 10058-F4 for 30 hr. The goat anti-c-MYC antibody and the rabbit anti-AO (A11) antibody were combined for the PLA, followed by incubation with Duolink® PLA anti-rabbit Plus (cat#DUO92002, Sigma-Aldrich) and anti-goat Minus probes (cat#DUO92006, Sigma-Aldrich). Of note, 1-Step Ultra TMB-ELISA Substrate Solution (cat#34029, ThermoFisher Scientific), instead of the precipitating substrate provided by the kit, was used for the substrate development.

Immunoblotting and Immunoprecipitation

Whole-cell protein extracts were prepared in cold cell-lysis buffer (50mM Tris-Cl, pH 7.5, 120mM NaCl, 0.5% NP-40 and 1mM PMSF). Proteins were transferred to nitrocellulose membranes. Following incubation with the blocking buffer (5% non-fat milk in 1x TBS-T) for 1 hour at RT, membranes were incubated with primary antibodies (1:1,000 dilution in the blocking buffer) overnight at 4 °C. After washing with 1xTBS-T for 3 times, membranes were incubated with peroxidase-conjugated secondary antibodies (1: 5000 diluted in the blocking buffer) at RT for 1 hr. Signals were detected using SuperSignal West chemiluminescent substrates (cat#34580 or 34095, Thermo Fisher Scientific Inc.).

For the A11 IP, HeLa cells were seeded for 24 hours or transfected with plasmid DNAs for 24 hours. Following trypsinization and washing in ice-cold 1xPBS, cells were lysed in cell lysis buffer on ice for 30 min and the extracts were centrifuged at 16,813×g for 5 min at 4°C to remove insoluble fractions. Soluble cell lysates (5 mg) were incubated with either rabbit IgG or anti-amyloid oligomers (A11) antibody (5 µg) at 4°C with gentle rotation for overnight. The immune complexes were then recovered with Dynabeads™ Protein G (cat#10004D, Life Technologies Corp.) or ChIP-Grade Protein G agarose beads (cat#9007S, Cell Signaling Technology). After washing with the lysis buffer, precipitates were subjected to SDS-PAGE and immunoblotting with either goat anti-c-MYC Abs or mouse anti-HA Abs, followed by incubation with HRP-conjugated bovine anti-goat IgG (cat#805-035-180, Jackson ImmunoResearch Laboratories Inc.) or EasyBlot® anti-mouse IgG (HRP) (cat#GTX221667-01, GeneTex Inc.). Signals were detected

using SuperSignal™ West Pico PLUS chemiluminescent substrates and documented with an iBright FL1000 Imaging System (ThermoFisher Scientific).

In Situ Proximity Ligation Assay (PLA)

The general procedures for *in situ* PLA were described previously.[15] For the specific MYC-A11 *in situ* PLA, the goat anti-c-MYC antibody and the rabbit anti-AO (A11) antibody were used, followed by incubation with Duolink® PLA anti-rabbit Plus and anti-goat Minus probes. Images were captured using a Zeiss LSM780 confocal microscope.

Brightfield *in situ* PLA was performed using the Duolink® In Situ Detection Reagents Brightfield. Paraffin-embedded tissue sections were deparaffinized at 60°C for 1.5 hr and rehydrated. Antigen retrieval was then performed using sodium citrate buffer (pH 6.0) in a vegetable steamer for 25 min. Following permeabilization using 0.3% Triton-X-100 in 1xPBS at RT for 10 min, endogenous peroxidase and alkaline phosphatase activities were quenched using the BLOXALL blocking solution at RT for 10 min and slides were blocked with 1x Duolink blocking solution (cat#DUO82007, Sigma-Aldrich) at 37°C for 1 hr. The tissue slides were incubated with rabbit anti-AO (A11) Abs (1:100) and goat anti-c-MYC Ab (1:100) or goat normal IgG (Jackson ImmunoResearch Labs) at RT for 3 hours, followed by incubation with anti-rabbit Plus and anti-goat Minus probes at 37°C for 1 hour, ligation at 37°C for 30 min, and amplification at 37°C for 100 min. After washing, the tissue sections were incubated with the detection reagent at RT for 1 hr, and the signals were developed with substrate at RT for 5 to 15 min and counterstained with nuclear staining solution. The slides were mounted for imaging.

In Vitro Fibrillation Assay

Reactions were carried out in non-binding black 96-well microplates (cat#655900, Greiner Bio-One North America Inc.). Each well contains 10 nM recombinant proteins or 100 nM c-MYC peptides with 10 μM Thioflavin T (ThT) in 1xPBS. Plates were incubated at 37°C with gentle shaking at 220 rpm in an Eppendorf ThermoMixer C (Eppendorf North America). ThT fluorescence was measured at Ex 450 nm/Em 500 nm using a CLARIOstar microplate reader (BMG LABTECH).

$A11^{+}$–AO ELISA

Following *in vitro* fibrillation assays, reaction solutions in multiple wells of 96-well microplates were collected and centrifuged at 10,000 rpm for 5 min. The collected supernatants were coated on 96-well UltraCruz® ELISA microplates (cat#sc-204463, Santa Cruz Biotechnology Inc.), 100 μl per well, at 4°C overnight. Plates were washed with 1xPBS and blocked with 5% nonfat milk in 1xTBS-T at RT for 1 hour. Following blocking, diluted A11 antibody (1:1000) in the blocking buffer was added 100 μl/well and incubated at 4°C overnight with gentle shaking. After washing with 1xTBS-T, each well was incubated with 100 μl of goat anti-rabbit IgG) poly-HRP conjugates (cat#PI32260, ThermoFisher Scientific, 1:1000 dilution in the blocking buffer) at RT for 1 hour. Following washing, 100 μl of 1-Step Ultra TMB-ELISA substrates was added to each well. The plates were incubated at RT on a shaker for 2-5 min, followed by measuring the OD at 650 nm using a SpectraMax iD5 multi-mode microplate reader (Molecular Devices).

Transmission Electron Microscopy

Recombinant proteins were first desalted and reconstituted in 1xPBS. Protein concentrations were adjusted to 0.5 μM with 1xPBS in 96-well non-binding microplates and incubated at 37°C with gentle shaking at 400 rpm in an Eppendorf ThermoMixer C (Eppendorf North America). Following incubation for 5 days, 10 μl of each reaction solution was applied on a piece of parafilm. Then, a water-treated 400-mesh carbon-coated copper grid (cat#CF400-Cu-50, Electron Microscopy Sciences Inc.) was immersed in the droplet of sample suspensions for 1 min, and the remaining liquid was wicked away. The grids were immediately incubated with a drop of 2% uranyl acetate solution (cat#22400-2, Electron Microscopy Sciences Inc.) for 1 min. After wicking, the grids were air-dried and examined under a Hitachi HT7800 transmission electron microscope (Hitachi, Ltd. Group, Japan) operating at 120 kV.

Transfection and c-MYC dual reporter assays

All plasmids were transfected with TurboFect™ transfection reagents (cat# R0531, Thermo Fisher Scientific). HeLa cells were co-transfected with pMYC-SEAP and pCMV-Gaussia luciferase (GLuc) reporter plasmids, along with various indicated plasmids for 24 hr. Reporter activities in culture media were measured. SEAP and GLuc activities in culture supernatants were quantitated using a NovaBright Phospha-Light EXP Assay Kit (cat# N10578, Thermo Fisher Scientific) for SEAP and a Pierce™ Gaussia Luciferase Glow Assay Kit (cat#16160, Thermo Fisher Scientific), respectively. Luminescence signals were measured by a CLARIOstar microplate reader (BMG LABTECH). SEAP activities were normalized against GLuc activities.

Detection of Apoptosis

NIH3T3 cells were seeded in 6-well culture plates and transfected with plasmid DNAs for 24 hours. The cell culture medium was refreshed with 0.5% serum-containing DMEM for 20 hours. Cells were then collected by trypsin-EDTA digestion, washed and fixed with 4% formaldehyde at RT for 30 min. Fixed cells were subsequently permeabilized with 0.3% Triton X-100 in 1xPBS at RT for 10 min. Following wash with 1xPBS, cell pellets were resuspended and incubated with 150 µL of rabbit anti-cleaved caspase-3 Abs (cat#9661, Cell Signaling Technology, 1:200 diluted with 5% BSA in 1xPBS) at 4°C overnight. Subsequently, cells were washed and incubated with Alexa Fluor 647-conjugated goat anti-rabbit IgG (H+L) (cat# A-21245, Thermo Fisher Scientific, 1:700 diluted with 5% BSA in 1xPBS) for 1h at RT. Following washing and resuspending in 1xPBS, cells were subjected to quantification by Flow Cytometry. For detection of Alexa Fluor 647, a BD LSRFortessa™ flow cytometer (BD Biosciences, San Jose, CA) with red laser excitation at 640 nm and emission detector bandpass filter of 670/30 nm was used. Data were collected using BD FACS Diva software version 8.0.1.

QUANTIFICATION AND STATISTICAL ANALYSIS

Statistical analyses were performed using Prism 10 (GraphPad Software). All results are expressed as mean±SD, mean±SEM, or median±IQR. The statistical significance is defined as: *$p<0.05$, **$p<0.01$; ***$p<0.001$; ****$p<0.0001$; n.s.: not significant. The *in vitro* and *ex vivo* experiments were not randomized.

REFERENCES

1. Dang CV. MYC on the path to cancer. Cell. 2012;149(1):22–35. doi: 10.1016/j.cell.2012.03.003. PubMed PMID: 22464321; PMCID: PMC3345192.
2. Okita K, Yamanaka S. Induced pluripotent stem cells: opportunities and challenges. Philos Trans R Soc Lond B Biol Sci. 2011;366(1575):2198–207. doi: 10.1098/rstb.2011.0016. PubMed PMID: 21727125; PMCID: PMC3130417.
3. Fernandez PC, Frank SR, Wang L, Schroeder M, Liu S, Greene J, Cocito A, Amati B. Genomic targets of the human c-Myc protein. Genes Dev. 2003;17(9):1115–29. Epub 20030414. doi: 10.1101/gad.1067003. PubMed PMID: 12695333; PMCID: PMC196049.
4. Blackwood EM, Eisenman RN. Max: a helix-loop-helix zipper protein that forms a sequence-specific DNA-binding complex with Myc. Science. 1991;251(4998):1211–7. doi: 10.1126/science.2006410. PubMed PMID: 2006410.
5. Vita M, Henriksson M. The Myc oncoprotein as a therapeutic target for human cancer. Semin Cancer Biol. 2006;16(4):318–30. Epub 20060803. doi: 10.1016/j.semcancer.2006.07.015. PubMed PMID: 16934487.
6. Hermeking H, Eick D. Mediation of c-Myc-induced apoptosis by p53. Science. 1994;265(5181):2091–3. doi: 10.1126/science.8091232. PubMed PMID: 8091232.
7. Hoffman B, Liebermann DA. Apoptotic signaling by c-MYC. Oncogene. 2008;27(50):6462–72. doi: 10.1038/onc.2008.312. PubMed PMID: 18955973.
8. Mitchell KO, Ricci MS, Miyashita T, Dicker DT, Jin Z, Reed JC, El-Deiry WS. Bax is a transcriptional target and mediator of c-myc-induced apoptosis. Cancer Res. 2000;60(22):6318–25. PubMed PMID: 11103792.
9. Eischen CM, Packham G, Nip J, Fee BE, Hiebert SW, Zambetti GP, Cleveland JL. Bcl-2 is

an apoptotic target suppressed by both c-Myc and E2F-1. Oncogene. 2001;20(48):6983–93. doi: 10.1038/sj.onc.1204892. PubMed PMID: 11704823.

10. Knowles TP, Vendruscolo M, Dobson CM. The amyloid state and its association with protein misfolding diseases. Nat Rev Mol Cell Biol. 2014;15(6):384–96. doi: 10.1038/nrm3810. PubMed PMID: 24854788.
11. Yakupova EI, Bobyleva LG, Vikhlyantsev IM, Bobylev AG. Congo Red and amyloids: history and relationship. Biosci Rep. 2019;39(1). Epub 20190115. doi: 10.1042/BSR20181415. PubMed PMID: 30567726; PMCID: PMC6331669.
12. Kayed R, Head E, Thompson JL, McIntire TM, Milton SC, Cotman CW, Glabe CG. Common structure of soluble amyloid oligomers implies common mechanism of pathogenesis. Science. 2003;300(5618):486–9. doi: 10.1126/science.1079469. PubMed PMID: 12702875.
13. Sanchez I, Mahlke C, Yuan J. Pivotal role of oligomerization in expanded polyglutamine neurodegenerative disorders. Nature. 2003;421(6921):373–9. doi: 10.1038/nature01301. PubMed PMID: 12540902.
14. Tang Z, Dai S, He Y, Doty RA, Shultz LD, Sampson SB, Dai C. MEK guards proteome stability and inhibits tumor-suppressive amyloidogenesis via HSF1. Cell. 2015;160(4):729–44. doi: 10.1016/j.cell.2015.01.028. PubMed PMID: 25679764; PMCID: PMC4564124.
15. Xu M, Lin L, Ram BM, Shriwas O, Chuang KH, Dai S, Su KH, Tang Z, Dai C. Heat shock factor 1 (HSF1) specifically potentiates c-MYC-mediated transcription independently of the canonical heat shock response. Cell Rep. 2023;42(6):112557. Epub 20230523. doi: 10.1016/j.celrep.2023.112557. PubMed PMID: 37224019; PMCID: PMC10592515.
16. Li J, Labbadia J, Morimoto RI. Rethinking HSF1 in Stress, Development, and Organismal

Health. Trends Cell Biol. 2017;27(12):895–905. Epub 20170907. doi: 10.1016/j.tcb.2017.08.002. PubMed PMID: 28890254; PMCID: PMC5696061.

17. Anckar J, Sistonen L. Regulation of HSF1 function in the heat stress response: implications in aging and disease. Annu Rev Biochem. 2011;80:1089–115. doi: 10.1146/annurev-biochem-060809-095203. PubMed PMID: 21417720.
18. Hegazy M, Cohen-Barak E, Koetsier JL, Najor NA, Arvanitis C, Sprecher E, Green KJ, Godsel LM. Proximity Ligation Assay for Detecting Protein-Protein Interactions and Protein Modifications in Cells and Tissues in Situ. Curr Protoc Cell Biol. 2020;89(1):e115. doi: 10.1002/cpcb.115. PubMed PMID: 33044803; PMCID: PMC8041061.
19. Yin X, Giap C, Lazo JS, Prochownik EV. Low molecular weight inhibitors of Myc-Max interaction and function. Oncogene. 2003;22(40):6151–9. doi: 10.1038/sj.onc.1206641. PubMed PMID: 13679853.
20. Augert A, Mathsyaraja H, Ibrahim AH, Freie B, Geuenich MJ, Cheng PF, Alibeckoff SP, Wu N, Hiatt JB, Basom R, Gazdar A, Sullivan LB, Eisenman RN, MacPherson D. MAX Functions as a Tumor Suppressor and Rewires Metabolism in Small Cell Lung Cancer. Cancer Cell. 2020;38(1):97–114 e7. Epub 20200528. doi: 10.1016/j.ccell.2020.04.016. PubMed PMID: 32470392; PMCID: PMC7363581.
21. Freie B, Ibrahim AH, Carroll PA, Bronson RT, Augert A, MacPherson D, Eisenman RN. MAX inactivation deregulates the MYC network and induces neuroendocrine neoplasia in multiple tissues. Sci Adv. 2025;11(17):eadt3177. Epub 20250425. doi: 10.1126/sciadv.adt3177. PubMed PMID: 40279415; PMCID: PMC12024646.
22. Tang Z, Su KH, Xu M, Dai C. HSF1 physically neutralizes amyloid oligomers to empower overgrowth and bestow neuroprotection. Sci Adv. 2020;6(46). Epub 20201111. doi:

10.1126/sciadv.abc6871. PubMed PMID: 33177089; PMCID: PMC7673739.

23. Ferrer I, Blanco R. N-myc and c-myc expression in Alzheimer disease, Huntington disease and Parkinson disease. Brain Res Mol Brain Res. 2000;77(2):270–6. doi: 10.1016/s0169-328x(00)00062-0. PubMed PMID: 10837922.
24. Ferrer I, Blanco R, Carmona M, Puig B. Phosphorylated c-MYC expression in Alzheimer disease, Pick's disease, progressive supranuclear palsy and corticobasal degeneration. Neuropathol Appl Neurobiol. 2001;27(5):343–51. doi: 10.1046/j.1365-2990.2001.00348.x. PubMed PMID: 11679086.
25. Lee HG, Casadesus G, Nunomura A, Zhu X, Castellani RJ, Richardson SL, Perry G, Felsher DW, Petersen RB, Smith MA. The neuronal expression of MYC causes a neurodegenerative phenotype in a novel transgenic mouse. Am J Pathol. 2009;174(3):891–7. Epub 20090122. doi: 10.2353/ajpath.2009.080583. PubMed PMID: 19164506; PMCID: PMC2665749.

Figure 1

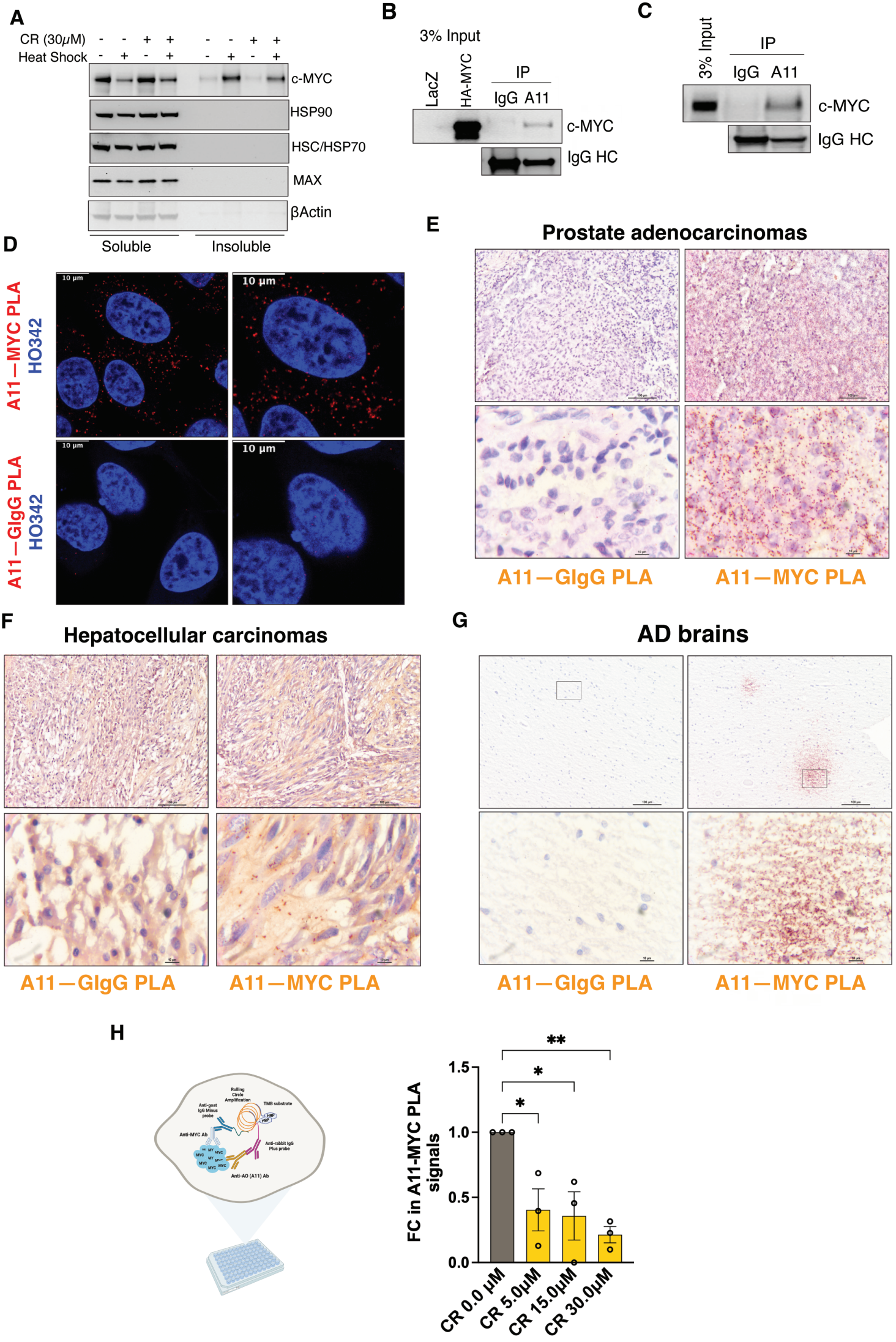
A
CR (30μM)
Heat Shock
c-MYC
HSP90
HSC/HSP70
MAX
βActin
Soluble
Insoluble
B
3% Input
LacZ
HA-MYC
IP
IgG A11
c-MYC
IgG HC
C
3% Input
IP
IgG A11
c-MYC
IgG HC
D
A11—MYC PLA
HO342
A11—GIgG PLA
HO342
10 μm
E
Prostate adenocarcinomas
A11—GIgG PLA
A11—MYC PLA
F
Hepatocellular carcinomas
A11—GIgG PLA
A11—MYC PLA
G
AD brains
A11—GIgG PLA
A11—MYC PLA
H
Rolling Circle Amplification
TMB substrate
Anti-goat IgG Minus probe
Anti-MYC Ab
Anti-rabbit IgG Plus probe
Anti-A0 (A11) Ab
FC in A11-MYC PLA signals
1.5
1.0
0.5
0.0
**
*
*
CR 0.0 μM
CR 5.0μM
CR 15.0μM
CR 30.0μM

FIGURE LEGENDS

Figure 1: c-MYC becomes detergent-insoluble and displays amyloid-like properties under proteotoxic stress and pathological conditions. (A) Detection of detergent-soluble and -insoluble c-MYC proteins by immunoblotting in HeLa cells pre-treated with 30 μM CR, followed by HS at 43ºC for 30 min (representative images of three independent experiments). (B) and (C) Immunoprecipitation of either exogenously expressed HA-c-MYC or endogenous c-MYC proteins in HeLa cells by A11 antibodies (representative images of three independent experiments). (D) Detection of endogenous c-MYC proteins in HeLa cells by PLA using both the goat anti-c-MYC Ab and the rabbit anti-AO (A11) Ab. Nuclei are counterstained with Hoechst 33342. Scale bar: 10 μm. (E)-(G) Detection of endogenous c-MYC proteins in human prostate adenocarcinoma, hepatocellular carcinoma, and Alzheimer's disease brain tissues by brightfield PLA using both the goat anti-c-MYC Ab and the rabbit anti-AO (A11) Ab. Scale bar: 100 μm for low magnification and 10 μm for high magnification. (H): Quantitation of endogenous c-MYC recognized by both the goat anti-c-MYC Ab and the rabbit anti-AO (A11) Ab through In-Cell PLA ELISA in HeLa cells treated with CR (mean ± SD, n=3 independent experiments, One-way ANOVA).

Figure 2

A

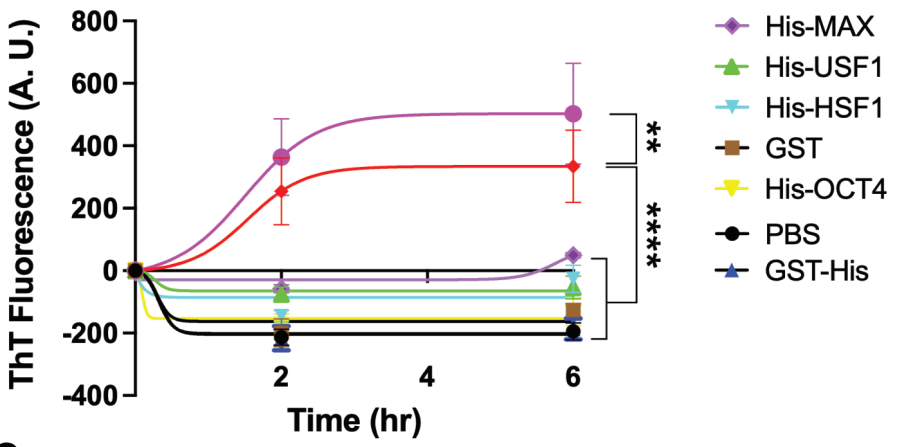

B

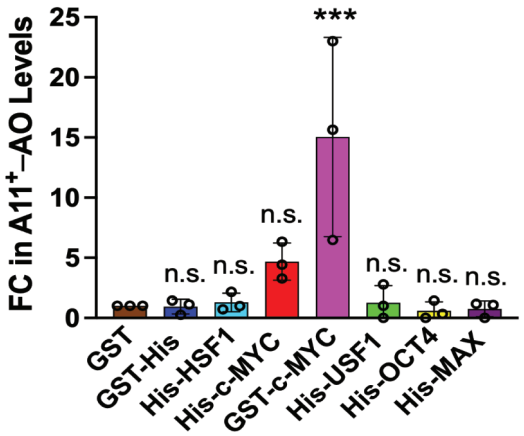

C

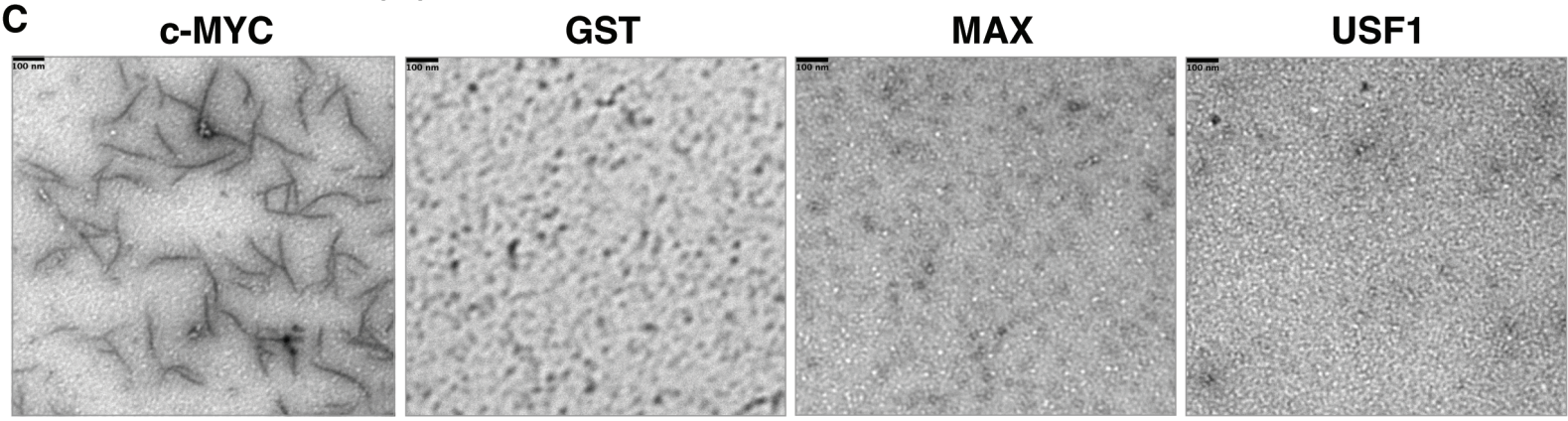

D

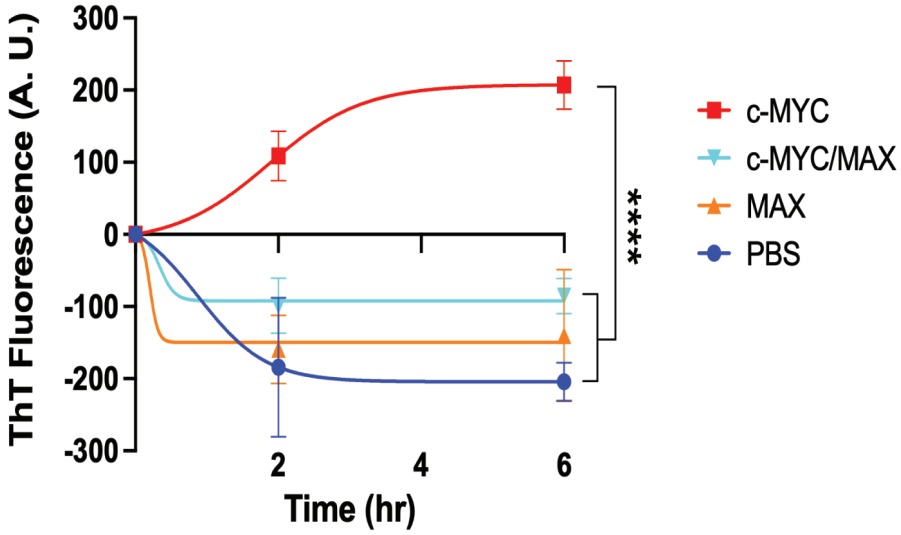

F

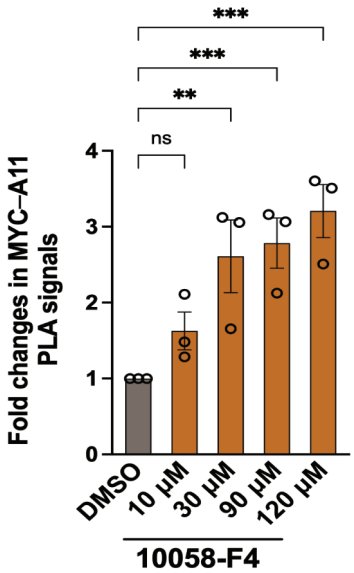

E

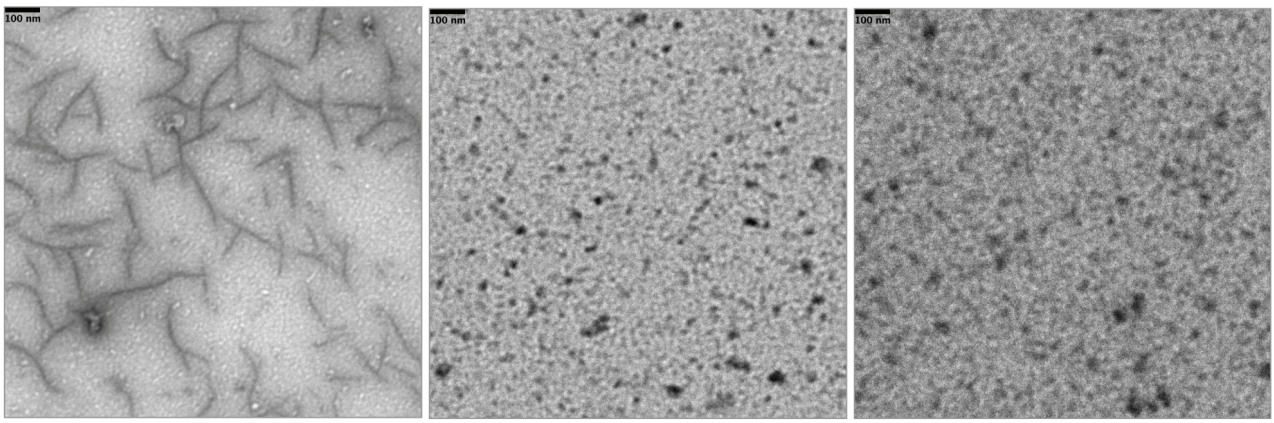

Figure 2: c-MYC is intrinsically amyloidogenic. (A) *In vitro* fibrillation assays using recombinant c-MYC proteins (mean ± SEM, n=3 independent experiments, Two-way ANOVA). (B) ELISA quantitation of $A11^{+}$–AOs generated by recombinant c-MYC proteins *in vitro* (mean ± SD, n=3 independent experiments, One-way ANOVA). (C) TEM visualization of protofibrils formed by recombinant c-MYC proteins *in vitro* (representative images of three independent experiments). Scale bars: 100 nm. (D) *In vitro* fibrillation assays using recombinant c-MYC /MAX dimers (mean ± SEM, n=3 independent experiments, Two-way ANOVA). (E) TEM visualization of recombinant c-MYC/MAX dimers *in vitro* (representative images of three independent experiments). Scale bars: 100 nm. (F) Quantitation of endogenous c-MYC AOs in HeLa cells treated with 10058-F4 by In-Cell PLA ELISA (mean ± SD, n=3 independent experiments, One-way ANOVA).

Figure 3

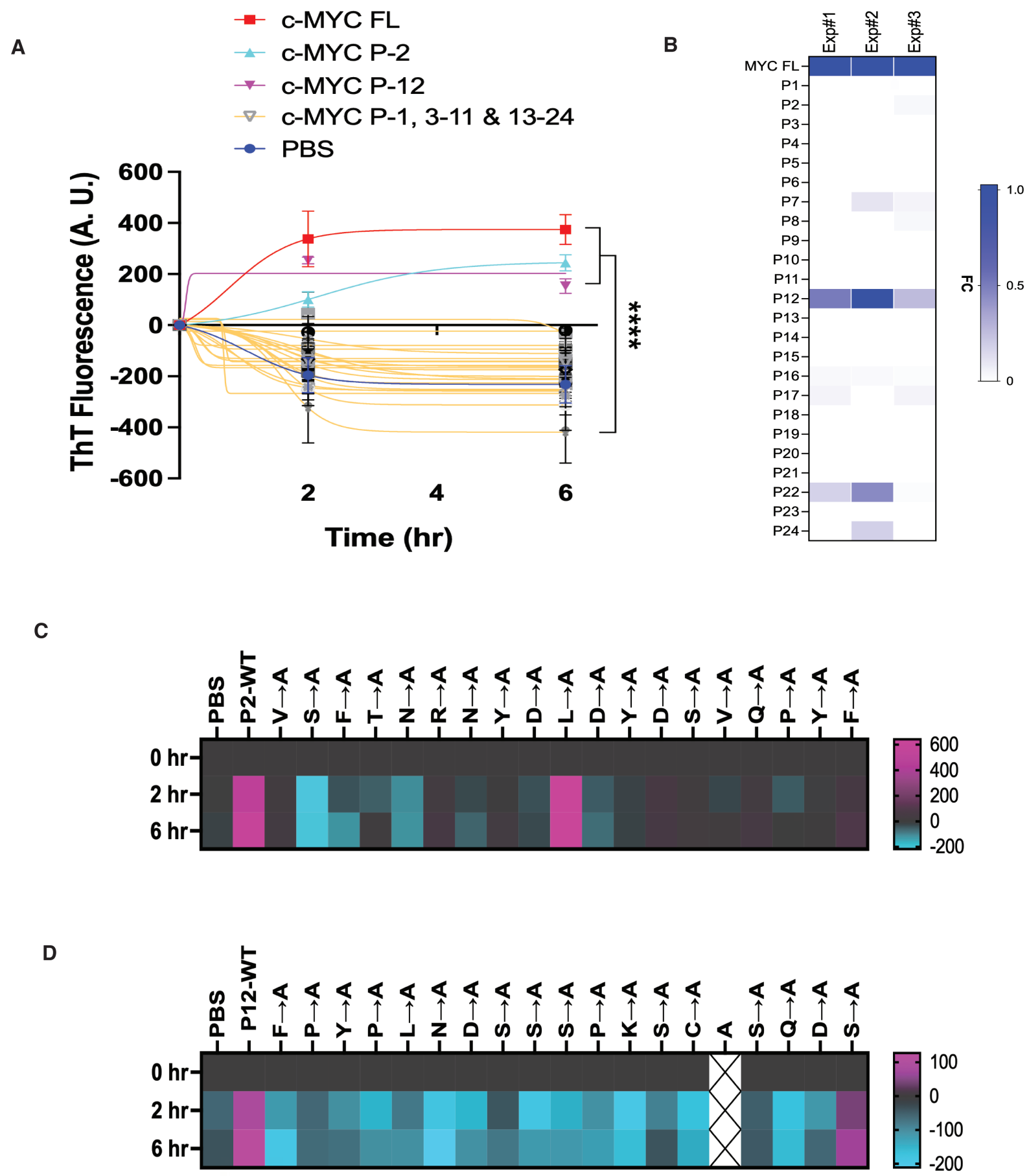
A
c-MYC FL
c-MYC P-2
c-MYC P-12
c-MYC P-1, 3-11 & 13-24
PBS
ThT Fluorescence (A. U.)
600
400
200
0
-200
-400
-600
2
4
6
Time (hr)
****
B
Exp#1
Exp#2
Exp#3
MYC FL
P1
P2
P3
P4
P5
P6
P7
P8
P9
P10
P11
P12
P13
P14
P15
P16
P17
P18
P19
P20
P21
P22
P23
P24
FC
1.0
0.5
0
C
PBS
P2-WT
V→A
S→A
F→A
T→A
N→A
R→A
N→A
Y→A
D→A
L→A
D→A
Y→A
D→A
S→A
V→A
Q→A
P→A
Y→A
F→A
0 hr
2 hr
6 hr
600
400
200
0
-200
D
PBS
P12-WT
F→A
P→A
Y→A
P→A
L→A
N→A
D→A
S→A
S→A
S→A
P→A
K→A
S→A
C→A
A
S→A
Q→A
D→A
S→A
0 hr
2 hr
6 hr
100
0
-100
-200

Figure 3: Decoding the amyloidogenicity of c-MYC *in vitro*. (A) *In vitro* fibrillation assays using the human c-MYC peptide library (mean ± SEM, n=3 independent experiments, Two-way ANOVA). (B) ELISA quantitation of $A11^{+}$–AOs generated by synthetic c-MYC peptides. Results of three independent experiments are presented as a heatmap. FC: fold change. (C) and (D) *In vitro* fibrillation assays using the P2 and P12 peptides that are subjected to alanine scan. Results are presented as heatmaps using the averages of three independent experiments.

Figure 4

A

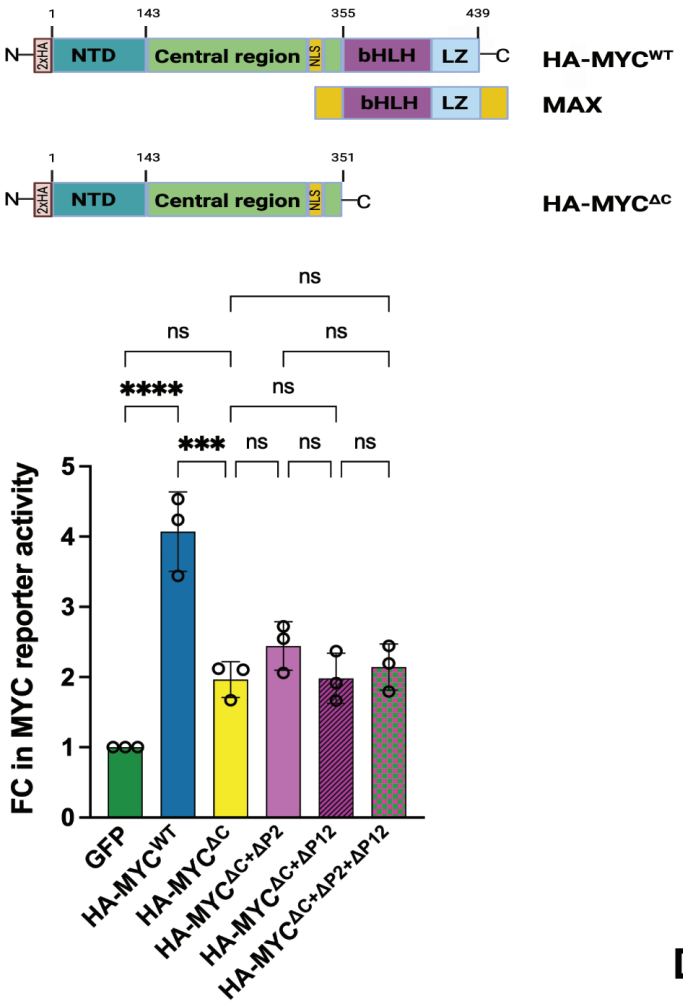

B

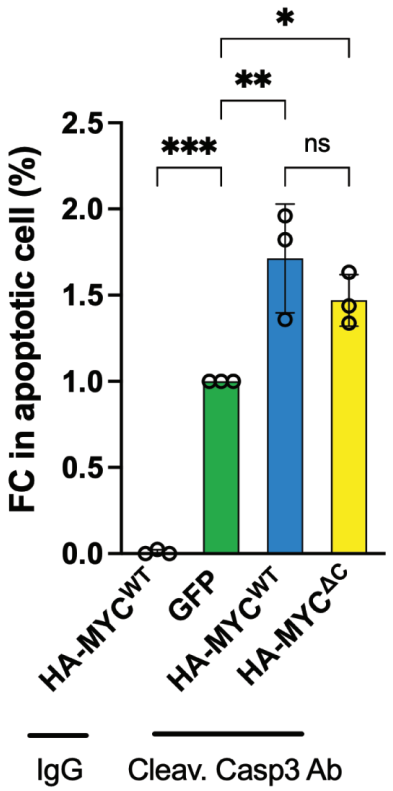

C

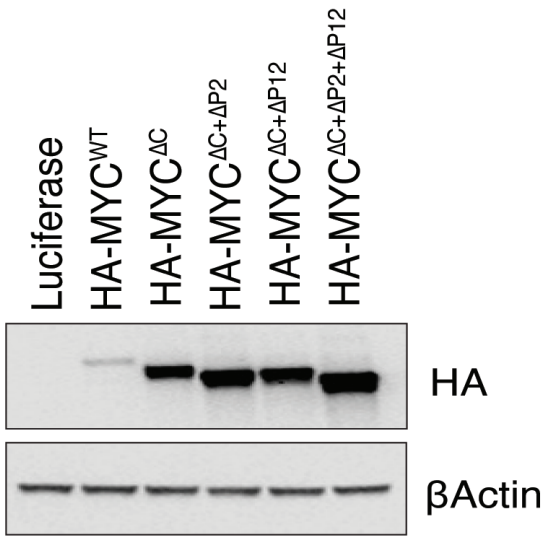

D

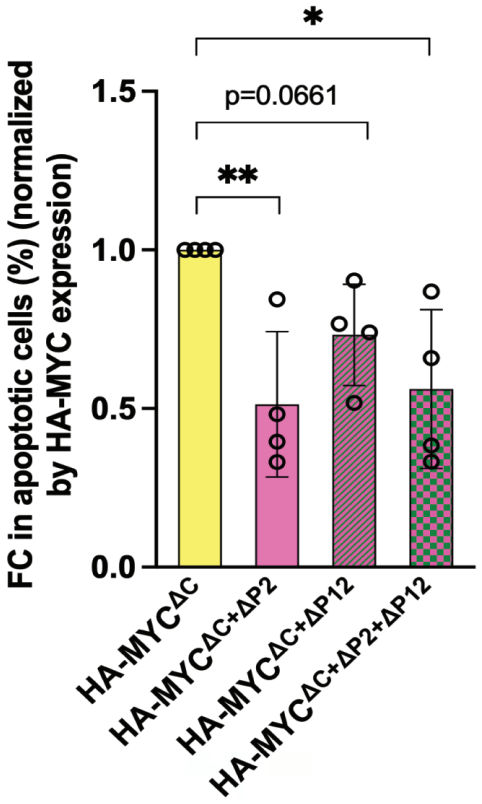

Figure 4: The amyloidogenesis of c-MYC contributes to its intrinsic tumor suppressor activity. (A) Measurements of the transcriptional activities of HA-MYC^{WT} and HA-MYC$^{\Delta C}$ in HeLa cells using the dual MYC reporter system (mean ± SD, n=3 independent experiments, One-way ANOVA). (B) Quantitation of apoptosis induced by transient expression of HA-MYC^{WT} or HA-MYC$^{\Delta C}$ in serum-starved NIH3T3 cells by flow cytometry using anti-cleaved caspase 3 Abs (mean ± SD, n=3 independent experiments, One-way ANOVA). (C) Detection of HA-MYC expression in serum-starved NIH3T3 cells by immunoblotting (representative images of four independent experiments). (E) Quantitation of apoptosis induced by transient expression of HA-MYC$^{\Delta C}$ and its deletion mutants in serum-starved NIH3T3 cells by flow cytometry using anti-cleaved caspase 3 Abs. The results are normalized by their expression levels (mean ± SD, n=4 independent experiments, One-way ANOVA).